Heterogeneous Catalysis

Deutsche Ausgabe: DOI: 10.1002/ange.201411581
Internationale Ausgabe: DOI: 10.1002/anie.201411581

Formation of a ZnO Overlayer in Industrial $Cu/ZnO/Al_2O_3$ Catalysts Induced by Strong Metal–Support Interactions

*Thomas Lunkenbein, Julia Schumann, Malte Behrens, Robert Schlögl, and Marc G. Willinger**

Abstract: *In industrially relevant $Cu/ZnO/Al_2O_3$ catalysts for methanol synthesis, the strong metal support interaction between Cu and ZnO is known to play a key role. Here we report a detailed chemical transmission electron microscopy study on the nanostructural consequences of the strong metal support interaction in an activated high-performance catalyst. For the first time, clear evidence for the formation of metastable "graphite-like" ZnO layers during reductive activation is provided. The description of this metastable layer might contribute to the understanding of synergistic effects between the components of the $Cu/ZnO/Al_2O_3$ catalysts.*

The activity of a heterogeneous catalyst depends on a perfect and optimized interplay of its microstructure and interface chemistry with the chemical potential of the environment. The investigation of sophisticated model catalysts is a general strategy to reduce the complexity of real systems.[1] However, careful investigations of realistic catalysts are still indispensable to countercheck the relevance of the proposed structural dynamics under real conditions.

For instance, methanol, a major industrial basic chemical, is obtained by the catalytic hydrogenation of CO and CO_2. Industrially relevant catalysts for methanol synthesis are composed of Cu (>50 mol %)/ZnO composites combined with a nonreducible oxide (≈ 10 mol %).[2] However, even 50 years after the first commercial use of Cu-based catalysts in methanol synthesis a comprehensive and widely accepted knowledge of the interplay between the involved components Cu, ZnO, and Al_2O_3 is still lacking.

Within the structure, ZnO stabilizes the Cu nanoparticles and induces a synergistic effect that tunes the catalyst. The latter can be explained by the appearance of strong metal support interaction (SMSI) and is difficult to study.[3] In one of the first studies tackling this interplay an oxide layer was proposed that embeds the Cu nanoparticles and increases the metal–oxide interface[4] which was confirmed by extensive studies tackling the SMSI effect on Cu-based model catalysts.[5] Recently, layers of a metastable "graphitic-like" (GL) form of ZnO_x were identified on the surface of an oxidized CuZn alloy.[1a] However, direct and visual evidence proofing the picture drawn by surface scientists for industrially relevant Cu/ZnO-based catalyst is still missing.

Here, we provide chemical electron microscopic insights on the formation of a metastable GL ZnO_x overlayer on Cu nanoparticles in an industrially relevant $Cu/ZnO/Al_2O_3$ catalyst. The appearance of this wetting oxide phase points to the origin of a self-assembled and efficient supply of the ZnO promoter on the Cu surface in Cu/ZnO-based catalysts. To study this interaction on a commercial $Cu/ZnO/Al_2O_3$ catalyst we followed the industrially applied recipe for high-performance catalysts[6] with a Cu-rich molar ratio of Cu/Zn of 70:30 in the presence of 1.5 mol-% of the structural promoter Al_2O_3.[2,7] Complementary catalytic tests further reveal high activity and decent stability in the synthesis of methanol from both, synthesis gas mixture and hydrogenation of CO_2 (Figure 1 A).

The microstructure of the fresh catalyst in the reduced state was first analyzed by high-angle annular dark field scanning transmission electron microscopy (HAADF-STEM, Figures 1 B,C and SI5). The images demonstrate that the Cu nanoparticles (highlighted in red) are homogeneously distributed within a porous ZnO (yellow) rod-like matrix allowing high mass transport to the active sites. In agreement with our previous results[8] aberration-corrected high-resolution TEM (HR-TEM, Figure 1 D) shows that the Cu nanoparticles are enriched in twins and high-energy steps at the surface.

The efficient dispersion of Cu nanoparticles and oxide as well as the defective nature of the Cu nanoparticles are a result of the applied catalyst synthesis protocol through a suitable mixed precursor phase.[6] For instance, comparable micro- and defect structures were also obtained in the case of Cu/MgO catalysts prepared by an analogous synthesis.[9] However, the catalyst based on MgO was shown to be a drastically inferior CO_2 hydrogenation catalyst. Hence, the important impact of ZnO on the catalytic activity is not only restricted to the formation of defective Cu nanoparticles or to an efficient stabilization of the Cu by the wurtzite-type ZnO matrix, but this oxide triggers also the appearance of the Cu–ZnO synergy and SMSI upon reduction in hydrogen.[3] The SMSI is initiated by the partial reduction of the oxidic support and can be expressed by electronic and/or morphological changes. In the former case, electrons are transferred from the oxidic support to the metal through the interface (Schottky barrier),[10] whereas for the latter situation an increase in

[*] Dr. T. Lunkenbein, J. Schumann, Prof. Dr. R. Schlögl, Dr. M. G. Willinger
Department of Inorganic Chemistry
Fritz-Haber-Institut der Max-Planck-Gesellschaft
Faradayweg 4–6, 14195 Berlin (Germany)
E-mail: willinger@fhi-berlin.mpg.de
Prof. Dr. M. Behrens
University of Duisburg-Essen; Faculty of Chemistry
Universitätsstrasse 7, 45141 Essen (Germany)
Prof. Dr. R. Schlögl
Department of Heterogeneous Reactions
Max-Planck-Institute for Chemical Energy Conversion
Stiftstrasse 34–36, 45470 Mülheim an der Ruhr (Germany)

Supporting information for this article is available on the WWW under http://dx.doi.org/10.1002/anie.201411581.

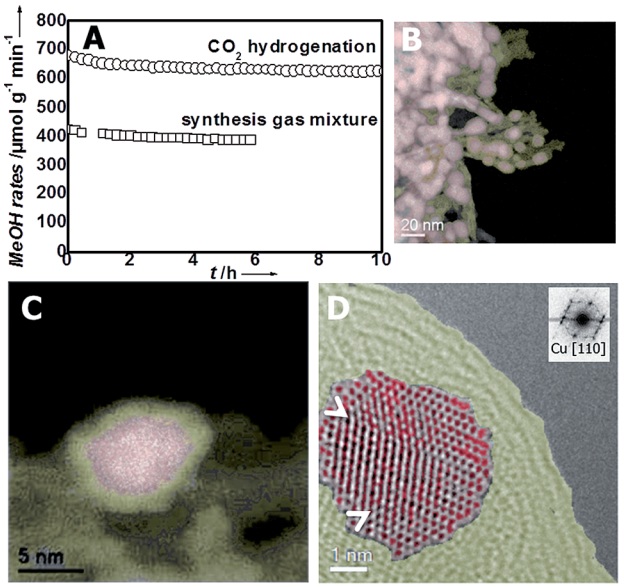

Figure 1. Characteristics of $Cu/ZnO/Al_2O_3$ catalyst. A) Methanol formation rate versus time for a synthesis gas mixture (squares) and CO_2 hydrogenation (circles) reaction at 230 °C, 30 bar, and differential conditions. B) and C) HAADF-STEM images of reduced $Cu/ZnO/Al_2O_3$ catalyst at different magnifications and areas. D) HRTEM image of $Cu/ZnO/Al_2O_3$ catalyst. The inset denotes a power spectrum, which allows to identify the Cu nanoparticle. The arrows in (D) mark twin boundaries. (All uncolored TEM images are present in the Supporting Information (Figures SI1–SI4).

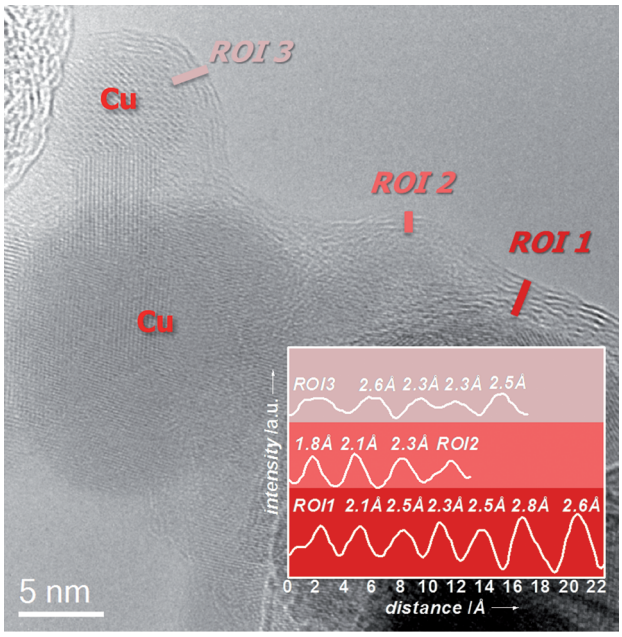

Figure 2. HRTEM micrograph of $Cu/ZnO/Al_2O_3$. The inset denotes the corresponding line scans taken from the assigned regions of interest (ROI).

adhesion is observed depending on the wetting affinity of the oxide.[11] In case of a mobile oxide, migration of the partially reduced oxide over the metal particle arises.[12] These possibilities are not mutually exclusive and can also be considered to appear simultaneously in a combination of embedding and local electronic perturbation.[13] The STEM images, however, clearly validate the wetting of the Cu nanoparticles within the industrial-type catalyst as SMSI-induced morphological change. In the HAADF-STEM images (Figures 1 B,C and SI5) the Cu nanoparticles are covered by a layer of reduced contrast (highlighted by a yellow envelope in Figure 1 B and C, see also shoulders in the line scan of Figure SI6) which appears slightly more intense in contrast compared to the stabilizing ZnO nanoparticles and indicates the embedding of the Cu nanoparticles. Additional STEM tilting series were recorded from −40° to +40° in α direction. The images reveal a complete coverage of the Cu nanoparticles by an overlayer of weaker contrast (movie M1). Furthermore, our HAADF-STEM pictures suggest that this morphological SMSI effect is a general feature of the reduced sample.

The HR-TEM micrographs in Figure 1 D and Figure 2 reveal atomic-scale details of the overgrowth. The images display a 1 to 2 nm thick layered material surrounding the nanoparticles which is comprised of four to six sheets with interlayer distances (d′) ranging from 1.8 Å to 2.8 Å (Figure 2). The broad d′ value distribution and the occurrence of interpenetrated layers is indicative for the presence of disorder within the layers. Interestingly, the measured d′ values are smaller compared to similar layered compounds, such as graphite (3.33–3.35 Å) or *h*-BN (3.30–3.33 Å).[14] We considered this layered overgrowth to be composed of ZnO as a metastable layered polymorph, such as summarized in Scheme 1 A (left). Layered or "graphitic" zinc oxide is not uncommon for thin ZnO films.[15] For thin ZnO_x films, this metastable polymorph exhibits a local minimum on the potential energy hypersurface separated by a small energy barrier from the thermodynamic stable wurtzite ZnO structure (Scheme 1 A, right).[15a] Crystallographically, the layered ZnO_x structure can be better described by the *h*-BN structure. In brief, the ZnO layers realize an AB stacking in which zinc is located on top of oxygen (Scheme 1 A, left) and each atom has a three-fold coordination.[15a] The d′ values correspond to the Zn–O distance along the crystallographic c-direction. In wurtzite ZnO the Zn–O distances equal 1.97 Å and 1.99 Å, respectively (Scheme 1 A, right). DFT calculations and surface X-ray diffraction experiment show that after the transformation to the "graphitic" or *h*-BN-type ZnO_x polymorph the intralayer distance (d) is decreased by 3 % to 1.92 Å. In addition, the d′ values depend on the substrate and can be increased to 2.1–2.4 Å.[15a,c] It was shown that thin ZnO films supported on single crystalline model substrates also exhibit a certain degree of corrugation.[15c] Here, we investigated a more complicated real catalyst system which gives rise to stronger variations in the d′ value due to the curved surface. The pseudo-spherical geometry, high-energy steps, and defects of the Cu nanoparticles allow the occurrence of different terminated surfaces, resulting in a variety of different surface energies.[8] This strongly influences the stability of the ZnO overlayer and leads to the observed corrugation and variation in the interlayer distance. Due to its appearance in the high-resolution TEM images, we have labeled the distorted ZnO overlayer as GL ZnO throughout the manuscript.

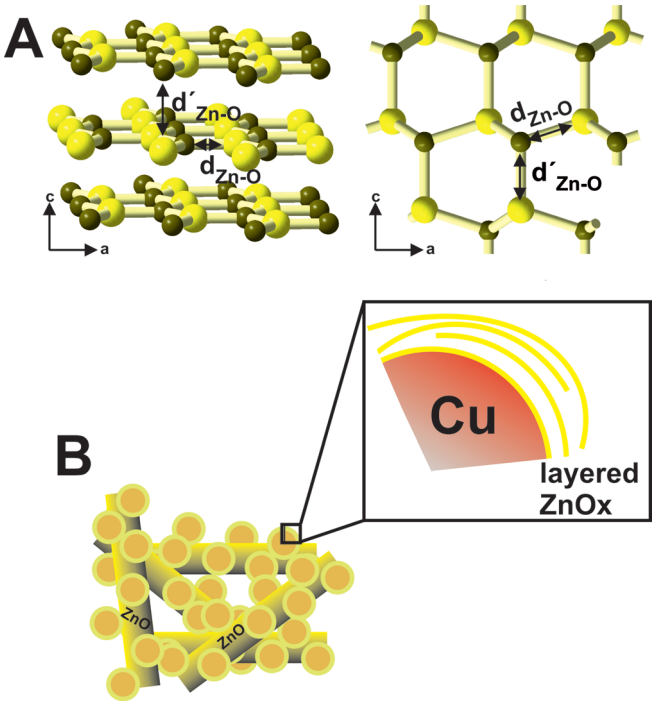

Scheme 1. A) Comparison of the graphitic and wurtzite ZnO polymorphs: ball-stick model of the ideal "graphitic" ZnO in the *h*-BN structure (modified from ICSD: 168894, left) and wurtzite ZnO viewed along the crystallographic *b* axis (ICSD: 26170, right). Small and large balls represent Zn and O atoms, respectively. B) Illustration of Cu/ZnO/Al_2O_3 after reduction in hydrogen. The inset emphasizes the distorted ZnO overlayer observed on the Cu particles.

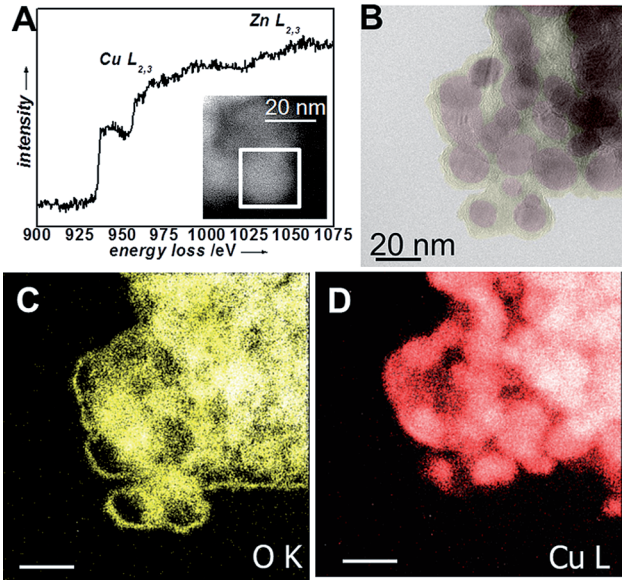

Figure 3. Analysis of the overgrowth. A) STEM-EELS-spectrum of Cu/ZnO/Al_2O_3 of the Cu $L_{2,3}$ and Zn $L_{2,3}$ edge of one single Cu nanoparticle. The inset denotes the corresponding HAADF-STEM image and the ROI from where the spectrum was collected. B) TEM image of the region where the EFTEM maps of (C) and (D) were recorded. C) and D) show oxygen K edge and copper L edge EFTEM maps of Cu/ZnO/Al_2O_3, respectively. The scale bars in (C) and (D) are 20 nm.

To confirm the presence of GL ZnO in the catalyst, a combined analysis of electron energy loss spectroscopy (EELS) and energy-filtered TEM (EFTEM) was conducted. For the EELS measurement (Figure 3A) the signal was acquired from individual Cu nanoparticles and their immediate surrounding (HAADF-STEM image in Figure 3A). The EELS spectrum represents the Cu $L_{2,3}$ and the Zn $L_{2,3}$ edges with absorption jumps at $E(Cu\,L_3) = 936$ eV, $E(Cu\,L_2) = 956$ eV, $E(Zn\,L_3) = 1027$ eV, and $E(Zn\,L_2) = 1046$ eV, respectively. The appearance of $L_{2,3}$ peaks is attributed to transitions from the 2p core levels to the unoccupied 3d levels.[16] In the Cu regime, no sharp peaks ("white lines") are observed, indicating fully occupied d-orbitals. Steps at 1027 eV and 1046 eV display the presence of Zn in the analyzed area, that is, in the vicinity of the Cu nanoparticles. However, Zn does not follow this white line argument, because it exhibits fully occupied d-orbitals in both oxidation states (0, +2). EFTEM maps of the oxygen K edge (Figure 3C) and Cu L edge (Figure 3D) were taken from the region shown in Figure 3B. The EFTEM maps indicate a core–shell morphology in which oxygen surrounds the Cu nanoparticles (see also Figure SI7). The EELS data reveals metallic Cu and the presence of zinc. Since there is no copper in the shell, it must consist of a zinc oxide layer on the Cu nanoparticles. Graphitic carbon can be excluded firstly by the oxygen map and secondly, the EELS spectrum of the C K edge recorded over the marked region in Figure SI8 does not show any signs of graphitic carbon.

The metastable nature of the layered and distorted ZnO_x overgrowth was finally evidenced by extended exposure of a Cu nanoparticle including the overlayer to the electron beam (Figure 4 and movie M2). Prolonged electron-beam irradiation induces morphological transitions of the metastable GL ZnO_x polymorph. The morphological and structural modification that was monitored by a series of HR-TEM images can be divided into three parts. First, the overgrowth starts to de-wet the surface of the Cu particle. Such behavior would not be expected for the case of a surface carbon layer for instance. Second, the metastable rock-salt ZnO polymorph crystallizes which, third, converts into the thermodynamically stable wurtzite ZnO structure after further beam irradiation. Electron beam exposure of the metastable ZnO_x thus helps to overcome the energy barrier between the

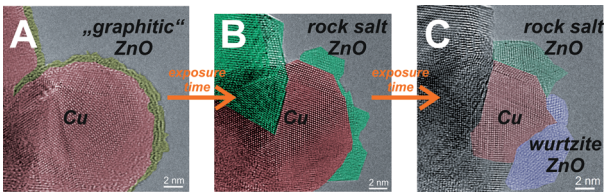

Figure 4. Transformation from graphitic-like ZnO_x to the wurtzite structure. A–C) HRTEM images of Cu/ZnO/Al_2O_3 after different times of electron beam exposure. For improved assignment of the lattice fringes, the particle in (C) was slightly tilted towards a zone axis of ZnO by 12°. The colors indicate the different state during phase transformation. The red-colored sites correspond to Cu particles. Yellow indicates graphitic-like ZnO_x. Green highlights the rock salt ZnO and blue regions correspond to the wurtzite ZnO structure.

different ZnO polymorphs and promotes the phase transformation. The transformation pathway GL–rock salt–wurtzite matches well with the theoretical expected reaction pathway through a cooperative process that involves a concerted movement of the atoms.[15a]

The presented data shows the occurrence of a layered ZnO overgrowth on Cu particles after reduction in hydrogen and is summarized in Scheme 1 B. The findings can be integrated into the long history of research on the understanding of Cu-based catalysts for methanol synthesis. Still, the nature of the active site is not clear. The reasons might be related to a complex and well-optimized interplay of the involved components among themselves and their dynamic responses to the applied chemical potential. For instance, the synergistic effect between the Cu and ZnO can be explained by the occurrence of a ZnO overlayer or by a surface alloy depending on the partial pressure or the nature of the reducing environment.[8,9,17] This proofs the chemical flexibility of the system. The presence of a ZnO overlayer after mild reduction conditions is in line with recent reports from Behrens et al.[8] and Zander et al.[9] Interestingly, although an almost complete Cu surface coverage is observed by TEM, the catalysts activity remains rather high. Note, in TEM imaging, only 2D projections are observed. Hence, it is difficult to draw conclusions on the accessibility of the complete Cu surface. In addition, the images show a distorted, corrugated, and partially interpenetrated overlayer rather than a well-ordered graphitic AB stacking, indicating the presence of a certain degree of porosity. In fact, Fichtl et al.[18] showed by H2-TPD measurements that roughly 30 % of the Cu surface area is accessible. This indicates that the high-performance catalyst for methanol synthesis breaks the direct correlation between surface area and activity. Furthermore, the formation of the overlayer demonstrates that ZnO, similar to Cu, exhibits a structural dynamic when exposed to different gaseous environment during reductive pretreatment.[19]

In summary, our results give clear evidence that activated high-performance Cu/ZnO catalysts carry a SMSI layer of metastable "graphitic-like" ZnO after reductive activation. The metastability was shown by giving a thermal stimulus with the electron beam resulting in a chain of structural transformations following the expectations from thermodynamics. The GL ZnO is kinetically stabilized by interacting with the defective and curved Cu surface underneath. Defects could play a role in the stability of the ZnO overlayer and may lead to the presence of some ZnO_x species acting as cocatalyst in the methanol synthesis. In addition, the overgrowth may protect the Cu from reshaping and sintering caused by the structural dynamics that are found for bare copper at variable chemical potential.[11] The synergy between Cu and ZnO is thus multiple with typical promoting functions for the active sites and with supporting and stabilizing functions for the mesostructure of the Cu phase. More work is needed to investigate the influence of the chemical potential during the methanol synthesis on the overgrowth. The present observations are ex situ and may only represent a still picture of a dynamic situation under working conditions. The present observations provide for the first time a direct and spatially resolved evidence for the proximity of the two synergistic components in the technical methanol synthesis catalyst. The present work may therefore serve as an example of how advanced chemical electron microscopy interacts with surface science model experiments and theory to elucidate the complex function of a high-performance catalyst that was initially found by empirical optimization.

Experimental Section

High-performance $Cu/ZnO/Al_2O_3$ catalysts were synthesized by coprecipitation as described elsewhere (FHI sample number: #15962, #15802).[2,7] Prior to the TEM measurements the calcined precursor was reduced in a hydrogen/argon mixture (20:80) at 250 °C for 90 min (heating rate: 1 °C min^{-1}) in a lockable reduction tube. For secure transfer to the TEM, the catalyst within the closed reduction tube was subsequently transferred into a glove box. Samples for TEM were prepared inside the glove box using lacey carbon-coated gold TEM grids. To exclude exposure to ambient air, samples were transferred into the microscope using a vacuum transfer holder (Gatan). Further details regarding the synthesis and the applied analytical techniques are summarized in the Supporting Information.

Keywords: electron microscopy · energy conversion · heterogeneous catalysis · methanol synthesis

How to cite: *Angew. Chem. Int. Ed.* **2015**, *54*, 4544–4548
Angew. Chem. **2015**, *127*, 4627–4631

[1] a) V. Schott, H. Oberhofer, A. Birkner, M. Xu, Y. Wang, M. Muhler, K. Reuter, C. Wöll, *Angew. Chem. Int. Ed.* **2013**, *52*, 11925–11929; *Angew. Chem.* **2013**, *125*, 12143–12147; b) M. G. Willinger, W. Zhang, O. Bondarchuk, S. Shaikhutdinov, H.-J. Freund, R. Schlögl, *Angew. Chem. Int. Ed.* **2014**, *53*, 5998–6001; *Angew. Chem.* **2014**, *126*, 6108–6112.

[2] M. Behrens, S. Zander, P. Kurr, N. Jacobsen, J. Senker, G. Koch, T. Ressler, R. W. Fischer, R. Schlögl, *J. Am. Chem. Soc.* **2013**, *135*, 6061–6068.

[3] a) S. J. Tauster, S. C. Fung, R. T. K. Baker, J. A. Horsley, *Science* **1981**, *211*, 1121–1125; b) S. J. Tauster, S. C. Fung, R. L. Garten, *J. Am. Chem. Soc.* **1978**, *100*, 170–175.

[4] J. C. Frost, *Nature* **1988**, *334*, 577–580.

[5] a) R. Naumann d'Alnoncourt, X. Xia, J. Strunk, E. Loffler, O. Hinrichsen, M. Muhler, *Phys. Chem. Chem. Phys.* **2006**, *8*, 1525–1538; b) E. V. Thomsen, M. Christiansen, J. Onsgaard, *Appl. Surf. Sci.* **1992**, *62*, 189–194; c) S. S. Fu, G. A. Somorjai, *Surf. Sci.* **1990**, *237*, 87–98; d) S. S. Fu, G. A. Somorjai, *Langmuir* **1992**, *8*, 518–524; e) S. S. Fu, G. A. Somorjai, *Appl. Surf. Sci.* **1991**, *48–49*, 93–103.

[6] M. Behrens, R. Schlögl, *Z. Anorg. Allg. Chem.* **2013**, *639*, 2683–2695.

[7] J. Schumann, T. Lunkenbein, A. Tarasov, N. Thomas, R. Schlögl, M. Behrens, *ChemCatChem* **2014**, *6*, 2889–2897.

[8] M. Behrens, F. Studt, I. Kasatkin, S. Kühl, M. Hävecker, F. Abild-Pedersen, S. Zander, F. Girgsdies, P. Kurr, B.-L. Kniep, M. Tovar, R. W. Fischer, J. K. Nørskov, R. Schlögl, *Science* **2012**, *336*, 893–897.

[9] S. Zander, E. L. Kunkes, M. E. Schuster, J. Schumann, G. Weinberg, D. Teschner, N. Jacobsen, R. Schlögl, M. Behrens, *Angew. Chem. Int. Ed.* **2013**, *52*, 6536–6540; *Angew. Chem.* **2013**, *125*, 6664–6669.

[10] a) J. A. Horsley, *J. Am. Chem. Soc.* **1979**, *101*, 2870–2874; b) B. H. Chen, J. M. White, *J. Phys. Chem.* **1982**, *86*, 3534–3541; c) J. M. Herrmann, *J. Catal.* **1984**, *89*, 404–412; d) A. Bruix, J. A. Rodriguez, P. J. Ramírez, S. D. Senanayake, J. Evans, J. B. Park,

D. Stacchiola, P. Liu, J. Hrbek, F. Illas, *J. Am. Chem. Soc.* **2012**, *134*, 8968 – 8974.
[11] P. L. Hansen, J. B. Wagner, S. Helveg, J. R. Rostrup-Nielsen, B. S. Clausen, H. Topsøe, *Science* **2002**, *295*, 2053 – 2055.
[12] a) J. Santos, J. Phillips, J. A. Dumesic, *J. Catal.* **1983**, *81*, 147 – 167; b) A. J. Simoens, R. T. K. Baker, D. J. Dwyer, C. R. F. Lund, R. J. Madon, *J. Catal.* **1984**, *86*, 359 – 372; c) H. R. Sadeghi, V. E. Henrich, *J. Catal.* **1984**, *87*, 279 – 282; d) A. K. Singh, N. K. Pande, A. T. Bell, *J. Catal.* **1985**, *94*, 422 – 435; e) T. Huizinga, H. F. J. van't Blik, J. C. Vis, R. Prins, *Surf. Sci.* **1983**, *135*, 580 – 596; f) A. D. Logan, E. J. Braunschweig, A. K. Datye, D. J. Smith, *Langmuir* **1988**, *4*, 827 – 830; g) Y. N. Sun, Z. H. Qin, M. Lewandowski, E. Carrasco, M. Sterrer, S. Shaikhutdinov, H. J. Freund, *J. Catal.* **2009**, *266*, 359 – 368.
[13] a) D. N. Belton, Y. M. Sun, J. M. White, *J. Am. Chem. Soc.* **1984**, *106*, 3059 – 3060; b) D. E. Resasco, G. L. Haller, *J. Catal.* **1983**, *82*, 279 – 288.
[14] O. Hod, *J. Chem. Theory Comput.* **2012**, *8*, 1360 – 1369.
[15] a) F. Claeyssens, C. L. Freeman, N. L. Allan, Y. Sun, M. N. R. Ashfold, J. H. Harding, *J. Mater. Chem.* **2005**, *15*, 139 – 148; b) C. L. Freeman, F. Claeyssens, N. L. Allan, J. H. Harding, *Phys. Rev. Lett.* **2006**, *96*, 066102; c) C. Tusche, H. L. Meyerheim, J. Kirschner, *Phys. Rev. Lett.* **2007**, *99*, 026102.
[16] V. J. Keast, A. J. Scott, R. Brydson, D. B. Williams, J. Bruley, *J. Microsc.* **2001**, *203*, 135 – 175.
[17] a) Z. Liu, A. Rittermeier, M. Becker, K. Kähler, E. Löffler, M. Muhler, *Langmuir* **2011**, *27*, 4728 – 4733; b) S. Kuld, C. Conradsen, P. G. Moses, I. Chorkendorff, J. Sehested, *Angew. Chem. Int. Ed.* **2014**, *53*, 5941 – 5945; *Angew. Chem.* **2014**, *126*, 6051 – 6055.
[18] M. B. Fichtl, J. Schumann, I. Kasatkin, N. Jacobsen, M. Behrens, R. Schlögl, M. Muhler, O. Hinrichsen, *Angew. Chem. Int. Ed.* **2014**, *53*, 7043 – 7047; *Angew. Chem.* **2014**, *126*, 7163 – 7167.
[19] a) T. W. Hansen, J. B. Wagner, P. L. Hansen, S. Dahl, H. Topsøe, C. J. H. Jacobsen, *Science* **2001**, *294*, 1508 – 1510; b) P. C. K. Vesborg, I. Chorkendorff, I. Knudsen, O. Balmes, J. Nerlov, A. M. Molenbroek, B. S. Clausen, S. Helveg, *J. Catal.* **2009**, *262*, 65 – 72; c) O. Martin, J. Perez-Ramirez, *Catal. Sci. Technol.* **2013**, *3*, 3343 – 3352.

Received: December 1, 2014
Published online: February 13, 2015

